NANO LETTERS

2008
Vol. 8, No. 1
195−202

CO Oxidation Catalyzed by Single-Walled Helical Gold Nanotube

Wei An, Yong Pei, and X. C. Zeng*

Department of Chemistry and Nebraska Center for Materials and Nanoscience, University of Nebraska—Lincoln, Lincoln, Nebraska 68588

Received September 19, 2007; Revised Manuscript Received November 16, 2007

ABSTRACT

We study the catalytic capability of unsupported single-walled helical gold nanotubes Au(5,3) by using density functional theory. We use the CO oxidation as a benchmark probe to gain insights into high catalytic activity of the gold nanotubes. The CO oxidation, catalyzed by the Au(5,3) nanotube, proceeds via a two-step mechanism, $CO + O_2 \rightarrow CO_2 + O$ and $CO + O \rightarrow CO_2$. The CO oxidation is initiated by the $CO + O_2 \rightarrow OOCO \rightarrow CO_2 + O$ reaction with an activation barrier of 0.29 eV. On the reaction path, a peroxo-type O–O–CO intermediate forms. Thereafter, the $CO + O \rightarrow CO_2$ reaction proceeds along the reaction pathway with a very low barrier (0.03 eV). Note that the second reaction cannot be the starting point for the CO oxidation due to the energetically disfavored adsorption of free O_2 on the gold nanotube. The high catalytic activity of the Au(5,3) nanotube can be attributed to the electronic resonance between electronic states of adsorbed intermediate species and Au atoms at the reaction site, particularly among the d states of Au atom and the antibonding $2\pi^*$ states of C–O and O1–O2, concomitant with a partial charge transfer. The presence of undercoordinated Au sites and the strain inherent in the helical gold nanotube also play important roles. Our study suggests that the CO oxidation catalyzed by the helical gold nanotubes is likely to occur at the room temperature.

1. Introduction. Gold is an inert metal in bulk form and possibly the noblest of all of the metals.[1] Unlike other transition-metal catalysts, gold had long been viewed as catalytically inactive. Since the pioneering work of Haruta and co-workers,[2a,b] many studies have demonstrated that nanogold can be a good catalyst for many important reactions[2c] such as CO oxidation,[2−20] epoxidation of propene,[21] selective or partial oxidation of methanol,[22a,b] and the water−gas shift reaction[22c−f] among others.[9] In particular, gold nanoparticles dispersed on a suitable oxide support can exhibit distinctive catalytic activity for CO oxidation at low temperature. Thus, nanogold catalysts can be applied for CO combustion in fuel cells or automobile emission control.

Many experimental efforts have been devoted to the understanding of the origin of high catalytic activity of nanogold and to improving the design of nanogold catalysts for better performance. Goodman and co-workers[3] suggested that the quantum size effects and factors such as the thickness, shape, and oxidation state of gold nanoparticles are responsible for the high catalytic activity of nanogold supported on TiO_2 (or Au/TiO_2) for CO oxidation. They observed 10 times higher activity for the CO oxidation on an atomically ordered bilayer structure of gold than that on the monolayer structure, as well as a reaction rate of more than 45 times faster than that on the most active Au/TiO_2 catalysts prepared via conventional synthesis methods. They also found that the reactivity decreases when the gold coverage exceeds two atomic layers.[3c] This intriguing catalytic behavior was later investigated by Hernández et al.[14a] and very recently by Rashkeev et al.[14b] using density functional theory. Wallace et al.[4] observed highly size-dependent reactivity for the coadsorption of CO and O_2 on gold anion clusters, as well as a phenomenon of cooperative coadsorption of CO and O_2 on Au_N^- clusters (N = even), that is, the presence of one preadsorbed adsorbate can enhance binding of another adsorbate. Haruta et al. reported a notable shape effect in which the catalytic performance of hemispherical gold nanoparticles is better than that of spherical particles.[2d] Landman and co-workers[5] revealed that the charging of a Au_8 cluster from oxygen-vacancy F-center defects of a MgO support plays a key role in the enhancement of catalytic activity. Other studies suggested that the oxygen vacancies formed at the interface of gold cluster/oxide support could contribute to the stabilization and activity of gold clusters on the support.[2c,6] Conversely, several groups showed that slightly oxidized gold ($Au^{+\delta}$) and metallic gold (Au^0) are crucial to high activity for dispersed gold catalyst.[7,8] Several studies indicated that the existence of water or hydroxyl groups can also enhance catalytic capability of nanogold for the CO oxidation.[10] For the oxide support, a general consensus has been that reducible (active) oxides such as TiO_2, CeO_2, or Fe_2O_3, which provide reactive oxygen species to redox cycle in the CO oxidation, are superior to nonreducible (inert) oxides such as MgO, Al_2O_3, or SiO_2

* To whom correspondence should be addressed. Email: xczeng@phase2.unl.edu.

10.1021/nl072409t CCC: $40.75 © 2008 American Chemical Society
Published on Web 12/21/2007

under similar catalytic conditions.[2b,5b,11,12] In any event, an oxide support is expected to have notable impact on the nanogold-catalyzed CO oxidation. A very recent study by Matthey et al.[13] reconfirms that gold nanoparticles dispersed on reducible oxides are better catalysts than those supported on nonreducible oxides, at least under high oxygen exposures. Moreover, these authors propose that the cationic state of gold ($Au^{+\delta}$) at the gold/support interface could be a generic system for catalytic reaction and that realistic reaction conditions should be taken into account when studying the oxidation state of gold in catalytic processes.

Many theoretical studies have also been devoted to gaining fundamental insights into the CO oxidation on supported or unsupported gold nanoclusters.[14−19] Hernández et al.[14a] attempted to elucidate the observed exceptional catalytic performance of the bilayer gold nanostructure.[3c] They concluded that the structural arrangement of the bilayer Au atoms on the surface of TiO_x/Mo(112) can better accommodate the synergistic reaction of the CO oxidation. Moreover, the higher electron density around the bottom Au layer can facilitate oxygen activation. The estimated activation barriers for the CO oxidation were 0.74, 0.29, and 0.45 eV when the Au coverage was 1, 4/3, and 5/2 ML, respectively. Very recently, Rashkeev et al. [14b] reported an even lower energy barrier (~0.1 eV) with the "magic" bilayer gold nanostructure. Molina et al.[15a] investigated the effect of modifying the interfacial perimeter of TiO_2(110)-supported Au aggregates on the O_2, CO adsorption, and the CO oxidation, respectively. They found that the CO oxidation near the edge sites of the Au particle entails a low reaction barrier (0.15 eV). Recently, Zhang et al.[16] also predicted the same barrier (0.15 eV) for the CO oxidation on Au/MgO/Mo(110).

Several theoretical studies have been reported on the catalytic capability of unsupported gold catalysts. Lopez and Nørskov[17a] revealed that the CO oxidation on an isolated Au_{10} cluster is via either the Langmuir−Hinshelwood or the Eley−Rideal mechanism. The reaction barrier associated with the CO oxidation is less than 0.4 eV. Liu et al.[18a] performed a DFT study of the CO oxidation catalyzed by various gold surfaces with or without defects. They found that the reaction proceeds more readily at the step sites rather than at the perfect sites. The CO oxidation at Au steps was predicated to have a reaction barrier of 0.46 eV. In general, the CO oxidation with a reaction barrier of less than 0.5 eV is expected to occur at the room temperature.

Several researchers[17−19] have emphasized that the presence of undercoordinated Au sites (e.g., defect sites) and strain are correlated with the high activity for the CO oxidation on supported or unsupported gold catalysts. Due to the complexity of the nanoparticle/support interaction, a complete understanding of the mechanism underlying the high catalytic capability of the Au/oxides system is still lacking. An unsupported gold catalyst is structurally self-supporting and thus less complicated. Thus, the relevant catalytic mechanism can be more easily understood. Recently, nanoporous gold foams have shown exceptional high catalytic activity for the CO oxidation, as good as the finely dispersed gold nanoparticles on a support.[20] The CO oxidation catalyzed by gold nanotube membranes at gas−water interfaces have also been shown to have reaction rates comparable to those on supported Au catalysts.[10a] These latest experimental findings have demonstrated that unsupported gold nanostructures can be alternative and effective catalysts.

As a novel form of gold nanostructures, single-walled helical gold nanotubes and multiwalled gold nanowires have been synthesized in the laboratory.[23] Theoretical studies of their geometric and electronic properties have been reported.[24] In this paper, we report, for the first time, a study of the catalytic capability of a prototype single-walled helical Au(5,3) nanotube using the CO oxidation as a benchmark probe. This gold nanotube can be also viewed as the thinnest gold nanowires (about 0.4 nm in diameter). Our calculations show that the activation barrier for the CO oxidation on a Au(5,3) nanotube is comparable to that on gold nanoclusters.

2. Models and Methods. In general, atomic geometries of gold nanotubes resemble those of carbon nanotubes but with a triangular network for gold rather than the hexagonal network for carbon. Hence, the chiral vector notation for carbon nanotubes C(*n*,*m*) can be also used for gold nanotubes, namely, Au(*n*,*m*). In this study, we will focus on a prototype helical nanotube, Au(5,3). The Au(5,3) nanotube is composed of five Au rows which coil around the nanotube axis with a helical pitch of 11 nm (Figure 1a).

The density functional theory (DFT) calculations were carried out using the DMol^3 package.[25] The spin-unrestricted DFT in the generalized gradient approximation with the Perdew−Burke−Ernzerhof (PBE) functional[26] was used to obtain all of the results presented in the next sections. The effective core potential (ECP) and a double numerical basis set including a d-polarization function (DND) were selected. Within the ECP scheme implemented in Dmol^3, all-electron calculations were performed for C and O atoms, and certain relativistic effects were included for Au atoms.

The hexagonal supercell for the Au(5,3) nanotube contains 43 gold atoms and has a dimension of 30 × 30 × 24.0 Å, where the length of *c* (24.0 Å) equals the periodicity of the Au(5,3) nanotube. The minimum distance between the sidewall of the Au nanotube and its periodic images is greater than 26.0 Å, which is sufficiently large to avoid the interaction between the nanotube and its periodic images. For geometry optimization and the search for the transition state (TS), the Brillouin zone integration was performed with the Γ point only, which yielded a 0.038 × 0.038 × 0.042 $Å^{-1}$ actual spacing. For calculation of the electronic properties, Monkhorst−Pack 1 × 1 × 6 *k*-points with 6 *k*-points along the nanotube axis were used,[27] and the real-space global orbital cutoff radius was set to be 6 Å. The minimum-energy pathway for elementary reaction steps was computed using the nudged elastic band (NEB) method.[28]

3. Results and Discussion. *3.1. Geometric and Electronic Properties of Au(5,3) Nanotubes.* As shown in Figure 1a, the optimized geometry of the Au(5,3) nanotube is a helical pentagonal tube with a circular top view in the axial direction. The coordination number of each Au atom is 6, indicating that any Au site on the Au(5,3) nanotube is undercoordinated

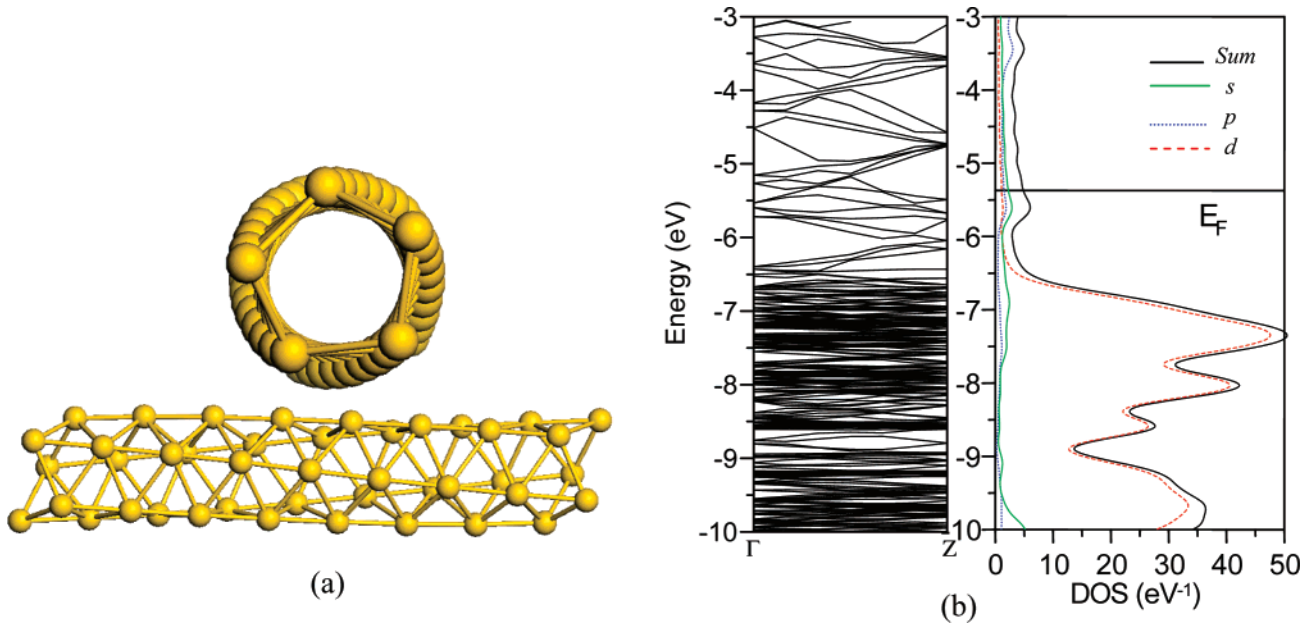

Figure 1. Geometric and electronic structures of the Au(5,3) nanotube. (a) Optimized geometry with top and side views displayed. (b) The electronic band structure and total density of states (DOS) including projected DOS onto s, p, and d orbitals of the pristine Au nanotube. E_F denotes the Fermi level at −5.37 eV.

compared to the bulk. Thus, all Au sites can be viewed as defect sites. Our calculation also shows that the *R* (right-handed) and *S* (left-handed) geometries of the Au(5,3) nanotube are almost isoenergetic. Here, we chose the (*R*)-Au(5,3) nanotube, which has been synthesized in the laboratory, as a model catalyst for the CO oxidation. The optimized (*R*)-Au(5,3) nanotube is 4.31 Å in diameter with a 22.45 Å helical pitch length (*L*/*n*) in one periodicity, which is in good agreement with the experimental measurements.[23b] The calculated Au−Au bond lengths are in the range of 2.80−2.91 Å, also in accordance with the measured values.[23a]

The appearance of helical morphology in tubular structures is not uncommon. Examples include single-walled carbon nanotubes, which may be either metallic or semiconducting, depending on the chirality of the nanotubes.[29] The electronic structures of Au(6,0), Au(7,3), and Au(8,4) nanotubes have been previously studied, and these tubes are all metallic, independent of the chirality.[24a] Our calculations of the electronic band structure and DOS for the Au(5,3) nanotube are consistent with previous results. As shown in Figure 1b, no band gap is seen near the Fermi level (E_F). Moreover, the α- and *β*-spin densities completely overlap, and no net spin DOS is observed, indicating that the Au(5,3) nanotube shows no magnetism. The total DOS below E_F from −6.5 to −10.0 eV are contributed mainly from the d-projected DOS, whereas the electronic states near E_F are mixed states with d as well as s and p characters.

3.2. Adsorption of O_2, CO, CO_2, and O. Two reaction mechanisms for the CO oxidation on nanogold are known,[14−19] (1) the Eley−Rideal (ER) mechanism, in which the gas-phase CO molecules directly react with activated O_2, i.e., adsorbed atomic O, where the activation of the O_2 molecule is the rate-limiting step, and (2) the Langmuir−Hinshelwood (LH) mechanism, in which the coadsorbed CO and O_2 molecules react to form a peroxo-type complex intermediate, which is the rate-limiting step. The first key issue therefore is to determine whether the CO oxidation is initiated via the ER or LH reaction route. Several studies have been devoted to this issue.[30−32] Theoretical calculations suggest that the enhancement in electron localization in small gold clusters can enhance O_2 binding.[30] Experimental studies of the TiO_2-(110)-supported gold clusters showed that the reduced Au nanoparticles can take part in the activation of O_2,[31a] and O vacancies of the support can assist in capturing gas-phase O_2 molecules.[31b,c] Several studies[10b,15b] also showed that O_2 can strongly bind to the O vacancy on the TiO_2(110) support, with an adsorption energy (E_{ad}) of −2.3 eV. For unsupported gold catalysts, however, a previous study showed that the lowest activation barrier is as high as 0.93 eV for the O_2 dissociation on a step edge (a defect site),[18a] thus ruling out the possibility of O_2 dissociation on unsupported gold catalysts at room temperature, although the O_2 dissociation could be greatly enhanced by the presence of some atomic oxygen.[32] On the other hand, Lopez and Nørskov[17a] reported that O_2 dissociation is extremely facile on an unsupported Au_{10} cluster.

Table 1. Adsorption Energy (E_{ad})[a] of Various Adsorbates on the Au(5,3) Nanotube and the Shortest Distance (*d*) between the Adsorbate and Sidewall of the Nanotube; Negative (Positive) E_{ads} Denotes Exothermic (Endothermic) Process

adsorbate	E_{ad} (eV)	*d* (Å)
CO	−0.72	1.97
O_2	0.34	2.28
CO_2	−0.04	3.44
O	−3.20	2.14
CO + O_2	−0.84	2.00(CO)/2.69(O_2)

[a] Adsorption energy is defined as $E_{ads} = E_{total}$[tube+adsorbate] − (E_{total}[tube] + E_{total}[adsorbate]), where E_{total} is the total energy of the system per supercell.

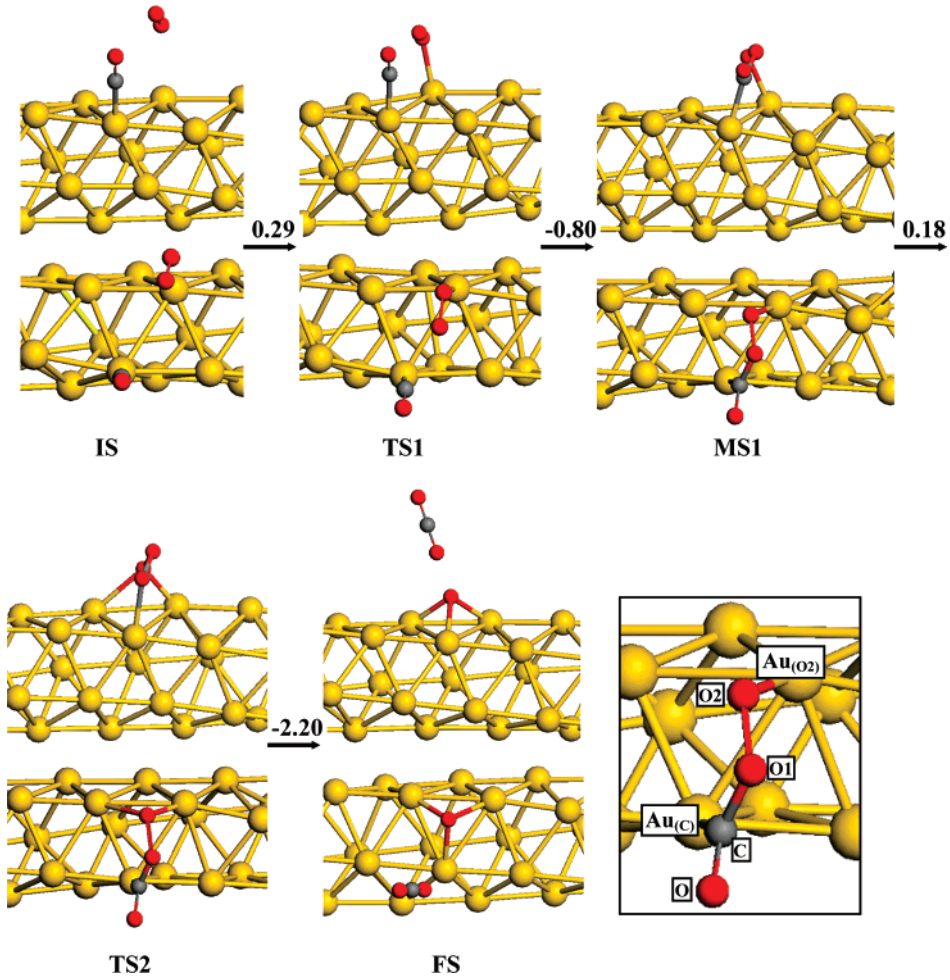

Figure 2. Local configurations of the adsorbates on the Au(5,3) nanotube at various intermediate states, including the initial state (IS), transition state (TS), metastable state (MS), and final state (FS) along the minimum-energy pathway via the CO + O_2 → OOCO → CO_2 + O route. Both side (upper panel) and top (lower panel) views are displayed, as well as the energy change (in eV) between neighboring states. The inset shows the elemental/label assignment listed in Table 2a.

Our calculation shows that the adsorption of O_2 on the Au(5,3) nanotube is endothermic (E_{ad} = 0.34 eV; see Table 1), supporting the conception that the O_2 adsorption on unsupported gold catalysts is energetically unfavorable. Consequently, the ER mechanism for the CO oxidation is unlikely with the unsupported Au(5,3) nanotube. Note that we examined many sites on the Au(5,3) nanotube in order to find out the most stable configuration for each adsorbate. For the CO adsorption, we found that E_{ad}(CO) is −0.72 eV, indicating that a CO molecule can be readily adsorbed onto the Au(5,3) tube at room temperature. There has been a report that E_{ad}(CO) is sensitive to the CO coverage.[18a] This coverage-dependent adsorption is not considered in this study. For CO_2, we found that $E_{ad}(CO_2)$ is −0.04 eV, suggesting that a CO_2 molecule is only physisorbed on the Au(5,3) tube and can also easily desorb from the reaction site at room temperature. As expected, the atomic O can strongly bind to the Au(5,3) nanotube with E_{ad}(O) = −3.20 eV, consistent with a previous study.[18a]

3.3. CO Oxidation. On the basis of the adsorption results, we studied the reaction mechanism for the CO oxidation on a Au(5,3) nanotube. We considered the LH reaction CO + O_2 → OOCO → CO_2 + O as a starting point, followed by the ER reaction CO + O → CO_2. To search for the minimum-energy pathway (MEP) for the CO oxidation, we selected an initial state (IS) configuration such that the O_2 is adsorbed on a Au atom with the CO molecule preadsorbed on a neighboring Au atom (Figure 2). The final state (FS) configuration is that a CO_2 molecule is physisorbed on the Au(5,3) tube with a chemisorbed atomic O nearby.

It is found that the presence of a preadsorbed CO on the neighboring Au atom notably enhances the binding of O_2 to the Au(5,3) nanotube, resulting in a net exothermic adsorption [E_{ad}(CO+O_2) = −0.84 eV]. Compared to the sum of the adsorption energies of O_2 and CO [0.34 + (−0.72) = −0.38 eV] (Table 1), the net increase in the binding energy for the coadsorption of O_2 and CO amounts to 0.46 eV, indicating a cooperative coadsorption of CO and O_2 can occur on the Au(5,3) nanotube.[4] This enhancement in the O_2 binding is partly due to the negatively charged neighboring Au atom (−0.1e) arising from a partial charge transfer from preadsorbed CO.

Next, we computed the MEP for the CO + O_2 → OOCO → CO_2 + O reaction using the NEB method. To achieve sufficient accuracy in calculating the MEP, 20 image structures were inserted between the IS and FS. The MEP

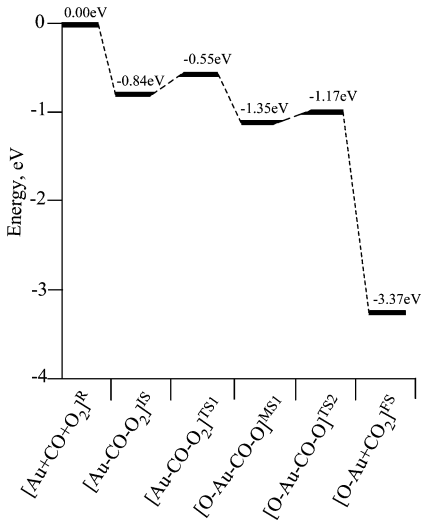

Figure 3. Schematic energy profile corresponding to local configurations shown in Figure 2 along the MEP via the CO + O_2 → OOCO → CO_2 + O route. All energies are given with respect to the reference energy, i.e., the sum of energies of the Au nanotube and individual CO and O_2 molecules.

profile is summarized in Figure 3. The energetics is schematically plotted with respect to the reference energy, which is the sum of the energies of the Au(5,3) nanotube and individual CO and O_2 molecules, assuming CO and O_2 are far apart. The local configurations of the adsorbates on the Au(5,3) nanotube at various states along the MEP are displayed in Figure 2, and the corresponding structural parameters are listed in Table 2a. The CO + O_2 reaction pathway features a peroxo-type O−O−C−O intermediate state, as marked by the metastable intermediate configuration (MS1).

Once CO and O_2 are coadsorbed on the Au(5,3) nanotube, the O_2 starts to approach CO at the reaction site to reach the first transition state (TS1). Both CO and O_2 are bonded with two neighboring Au atoms in this (net) endothermic process, imposing an energy barrier of 0.29 eV along the reaction pathway. Passing over TS1, a peroxo-type O2−O1-C−O complex (MS1) is formed, which is 0.80 eV lower in energy than TS1. Next, the O−O bond length d_{O1-O2} in the O2−O1-C−O complex is continually elongated from 1.463 to 1.796 Å, at which the system reaches the second transition state (TS2). Passing over TS2 with a relatively low barrier of 0.18 eV, a CO_2 molecule is formed, leaving an atomic O adsorbed on the threefold hollow site of the Au(5,3) nanotube. As mentioned in section 3.2, the CO_2 may easily desorb from the reaction site at room temperature due to the weak interaction between CO_2 and the Au(5,3) nanotube. The formation of the peroxo-type O−O−C−O complex along the reaction pathway has been confirmed experimentally by using vibrational spectroscopy measurements.[33]

We also examined whether the ER mechanism is conceivable after the CO_2 molecule is formed via the LH mechanism. A configuration of physisorbed CO above an O atom preadsorbed on the Au(5,3) nanotube was chosen as the IS (Figure 4 and Table 2b). It was found that a very small barrier (0.03 eV) separates the IS and the MS along the MEP. Note

Table 2. Structural Parameters for the Intermediate States along the Minimum Energy Pathway for the CO Oxidation on the Au(5,3) Nanotube: (a) CO + O_2 → OOCO → CO_2 + O;[a] (b) CO + O → CO_2.[a,b] Net Partial Charge Transfer (δq)[c] of the C Atom, and the Au Atom with the Shortest Distance from the C or O2 is Listed

(a)	IS	TS1	MS1	TS2	FS
$d_{(C-O)}$	1.147	1.151	1.207	1.220	1.175
$d_{(C-Au)}$	1.995	1.984	2.081	2.118	5.089
$d_{(C-O1)}$	3.495	2.531	1.369	1.288	1.174
$d_{(O1-O2)}$	1.240	1.281	1.463	1.796	3.735
$d_{(O2-Au)}$	2.688	2.216	2.270	2.136	2.137
∠(O−C−O1)	83.6	99.1	117.9	126.9	180.0
δq [C]	0.394	0.401	0.515	0.526	0.470
δq [$Au_{(C)}$]	−0.098	−0.083	−0.091	−0.090	
δq [$Au_{(O2)}$]	0.015	0.050	0.084	0.128	0.143

(b)	IS	TS	MS	FS
$d_{(C-O)}$	1.144	1.166	1.201	1.176
$d_{(C-Au)}$	4.137	2.248	2.088	3.687
$d_{(C-O2)}$	3.216	2.232	1.342	1.176
$d_{(O2-Au)}$	2.137	2.118	2.137	4.041
∠(O−C−O2)	93.1	113.5	127.3	180.0
δq [C]	0.011	0.262	0.624	0.472
δq [$Au_{(C)}$]	0.128	0.004	−0.096	
$<\delta q>$ [$Au_{(O2)}$]	0.140	0.129	0.096	

[a] The units of the bond distance and angle are Å and degrees (°), respectively. The unit of charge transfer is *e*. IS, TS1, MS1, TS1, and FS are displayed in Figure 2. [b] IS, TS, MS, and FS are displayed in Figure 4. [c] Charge transfer is calculated using the Mulliken charge analysis. Negative (positive) δq denotes charge gain (loss). $<\delta q>$[$Au_{(O2)}$] denotes mean charge transfer among the two Au atoms adjacent to O2.

that once the CO_2 molecule is formed via the LH mechanism and leaves the reaction site thereafter, a second CO molecule can be readily adsorbed on the same site to react with the atomic O on the Au(5,3) nanotube to form the second CO_2. The latter will also desorb from the sidewall of the Au(5,3) nanotube at room temperature.

In summary, the CO oxidation on the Au(5,3) nanotube can be characterized as a two-step process; the LH reaction initiates the CO oxidation followed by the ER reaction. Both reactions are likely to proceed at room temperature because of the low activation barriers involved.

3.4. Electronic Structure of Intermediate State for CO Oxidation. As mentioned in section 3.1, an infinitely long Au(5,3) nanotube (0.4 nm in diameter) is metallic, whereas finite-sized Au clusters supported on TiO_2 (Au/TiO_2) are nonmetallic if cluster sizes are less than 3 nm.[3a] Thus, the high catalytic activity of the Au(5,3) nanotube for the CO oxidation can be attributed to its unique helical geometry with undercoordinated Au sites in a strained state. To gain more insight into the origin of the high activity of the Au(5,3) nanotube, we illustrate the local density of states (LDOS) projected onto C−O (left panel in Figure 5) and O1−O2 (right panel in Figure 5), as well as the s-, p-, and d-projected LDOS of the Au atom that has the shortest distance from the C or O2 atom in the IS, TS1, and MS1, respectively (see the inset in Figure 2 for the atom labeling).

For the C−O species on the Au(5,3) nanotube shown in Figure 2, it can be seen that the initial (IS) empty antibonding

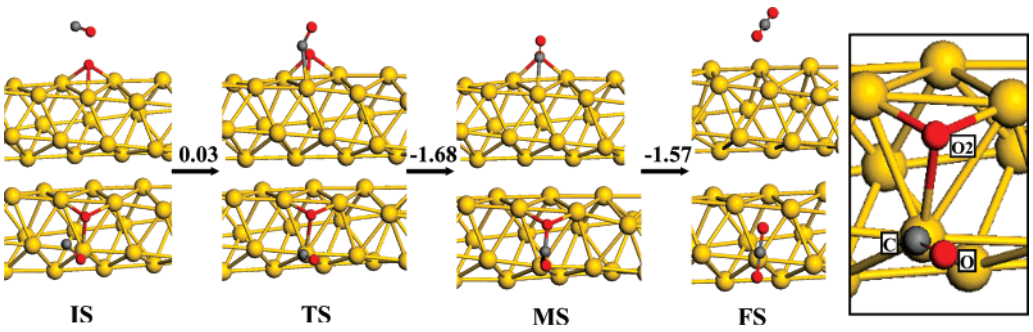

Figure 4. Local configurations of the adsorbates on the Au(5,3) nanotube at various intermediate states along the minimum-energy pathway via the CO + O → CO_2 route. Both side (upper panel) and top (lower panel) views are displayed, as well as the energy change (in eV) between neighboring states. The inset shows the elemental/label assignment listed in Table 2b.

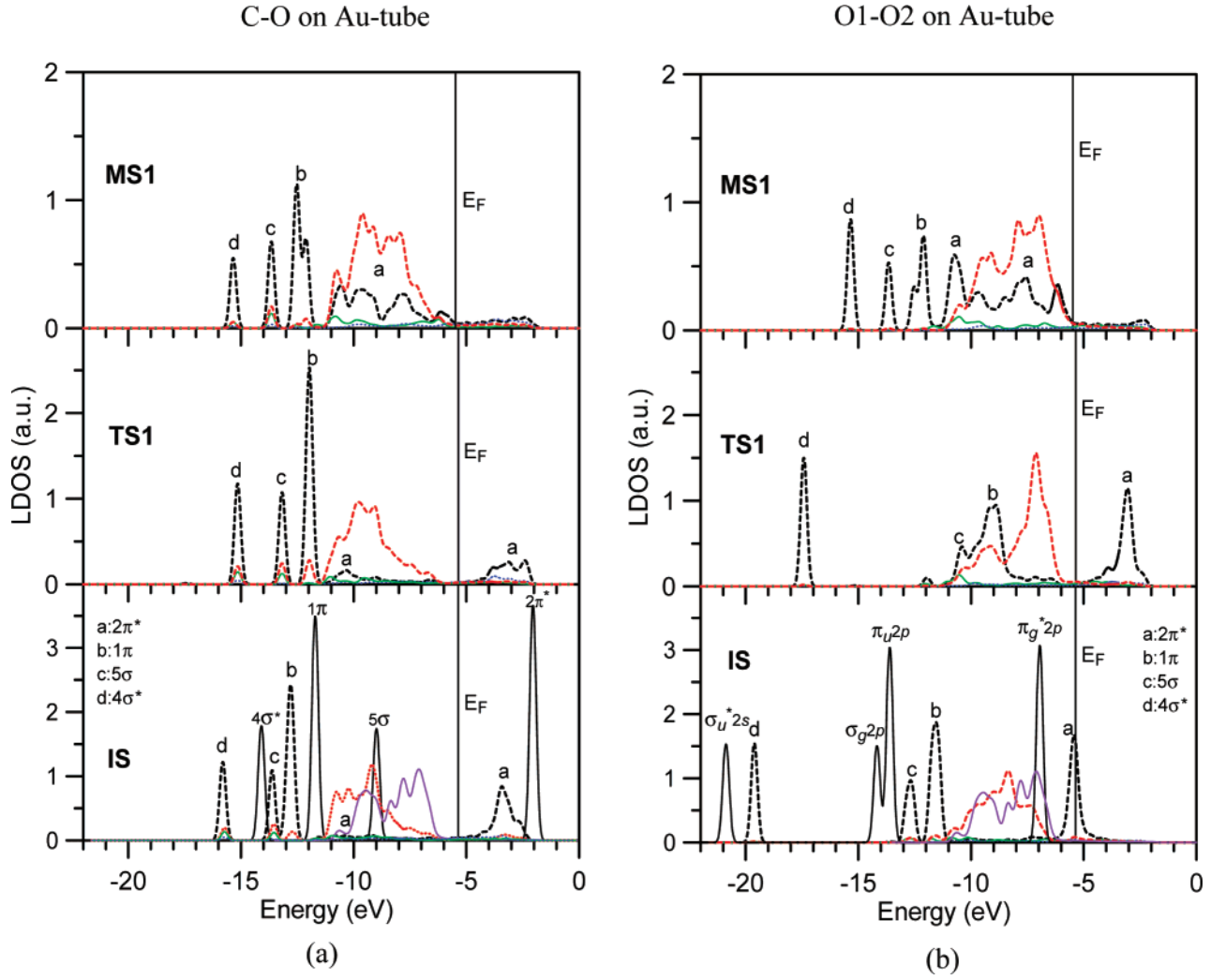

Figure 5. Local density of states (LDOS) projected onto (a) C−O and (b) O1−O2 on the Au(5,3) nanotube (Figure 2), together with the s-, p-, and d-projected LDOS of the Au atom in the IS, TS1, and MS1. E_F denotes the Fermi level, which is −5.36, −5.35, and −5.49 eV for the IS, TS1, and MS1, respectively. The homonuclear orbital notations are assigned only to the gas-phase O_2; black — gas-phase CO or O_2; black - - - C−O or O1−O2 on the Au nanotube; purple — d-projected LDOS of the pristine Au(5,3) nanotube; green —, blue · · ·, and red - - - s-, p-, and d-projected LDOS of the Au atom with the shortest distance from the C or O_2 atom.

orbital $2\pi^*$ of the gas-phase CO is pulled below the Fermi level (E_F) at MS1, and it is partially populated due to back-donation of d electrons and the electronic resonance between the antibonding $2\pi^*$ state of C−O and the d state of the $Au_{(C)}$ atom, as indicated by the slight increase in C−O bond length (see Table 2a). However, the substantial interaction between the d state of the Au atom [of the pristine Au(5,3) nanotube] and the nonbonding 5σ (carbon lone-pair electrons) state of the gas-phase CO leads to net partial charge transfer (δq; see Table 2a) from C−O to $Au_{(C)}$ in the IS, TS1, and MS1, rendering $Au_{(C)}$ with a net negative charge (∼ −0.1e). This interaction also shifts the 5σ states of the CO to lower

energy, even below the 1π state. Note that unlike Au atoms on a defective support which often bears a net partial charge,[18a] all Au atoms of the pristine Au(5,3) nanotube are charge neutral.

For O1−O2 species on the Au nanotube (Figure 2), it can be seen that, from IS to TS1, the half-occupied antibonding orbital π_g*2p of the gas-phase O_2 is elevated above the E_F due to the interaction between the d state of the Au atom [of the pristine Au(5,3) nanotube] and the antibonding π_g*2p state of the O_2. A charge depletion (positive δq) of $Au_{(O2)}$ occurs because the atomic O is more electronegative (Table 2a). As expected, the antibonding 4σ* (oxygen lone-pair) state is not involved in the reaction due to its position far below E_F. In contrast, the 2π* as well as the 1π and 5σ states of O1−O2 are more involved in the weakening of the O1−O2 bond in TS1 and MS1.

Overall, the formation of the labile peroxo-type O2−O1−C−O complex results in a redistribution of the LDOS and an orbital shift for both C−O and O1−O2 species. From the IS to TS1 to MS1, the 2π* states of C−O and O1−O2 spread back and forth over the Au d state (below E_F). Moreover, the states of C−O and O1−O2 interact with each other while the C−O1 bond is strengthening (forming) and the O1−O2 bond is weakening (breaking), as indicated by the increase in δq[C] (see Table 2a) as well as the superposition of the C−O and O1−O2 states at MS1 (Figure 5). In addition, the d states (red curves in Figure 5) rather than the s/p states of the Au atoms dominate the interaction between CO + O_2 and the Au(5,3) nanotube.

For the ER reaction, $Au_{(C)}$ in the IS and TS is partially positively charged (Table 2b) due to electron pulling from O2 which is prebonded at the threefold hollow site. Our calculation shows that the ER reaction can be even faster than the LH reaction if the gas-phase O_2 molecule can dissociate into atomic O first. This view is in accordance with previous findings that slightly oxidized gold ($Au^{+\delta}$) is crucial to achieve high activity for the dispersed Au clusters.

4. Conclusions. Using density functional theory, we investigate the reaction mechanism of CO oxidation catalyzed by the helical Au(5,3) nanotube, as well as structural and electronic properties of adsorbates and adsorbents. We find that the Au(5,3) nanotube exhibits high catalytic activity for the CO oxidation. The catalytic process is likely to proceed via a two-step mechanism, (1) LH, CO + O_2 → OOCO → CO_2 + O and (2) ER, CO + O → CO_2. The ER mechanism is ruled out as the starting point for the CO oxidation because direct adsorption of gas-phase O_2 on the Au(5,3) nanotube is energetically unfavorable. The CO oxidation on the Au(5,3) nanotube is most likely to proceed with the LH reaction due to cooperative coadsorption of CO and O_2 exothermically. On the reaction pathway, a peroxo-type O−O−C−O complex features the transition state and metastable state with a low activation barrier of 0.29 eV. Following the LH reaction, the ER reaction can then proceed with a much small barrier (0.03 eV). On the basis of the calculation, we predict that both routes (1) and (2) are fast reactions, and the CO oxidation on the Au(5,3) nanotube could occur at room temperature. The high catalytic activity of the Au(5,3) nanotube for the CO oxidation may be due to the presence of undercoordinated Au sites in the helical geometry. On the microscopic level, the high activity may be attributed to the electronic resonance among electronic states of C−O, O1−O2, and Au atoms, particularly, among the d state of the Au atom at the reaction site and the antibonding 2π* states of CO and O_2, concomitant with partial charge transfer.

Acknowledgment. This research was supported, in part, by grants from DOE (DE-FG02-04ER46164), NSF (CHE-0427746 and CHE-0701540), the Nebraska Research Initiative, and by the Research Computing Facility at the University of Nebraska—Lincoln.

References

(1) Hammer, B.; Nørskov, J. K. *Nature* **1995**, *376*, 238.
(2) (a) Haruta, M.; Kobayashi, T.; Samo, H.; Yamada, N. *Chem. Lett.* **1987**, 405. (b) Haruta, M.; Yamada, N.; Kobayashi, T.; Iijima, S. *J. Catal.* **1989**, *115*, 301. (c) Haruta, M. *Catal. Today* **1997**, *36*, 153. (d) Haruta, M. *CATTECH* **2002**, *6*, 102. (e) Haruta, M.; Tsubota, S.; Kobayashi, T.; Kageyama, H.; Genet, M. J.; Delmon, B. *J. Catal.* **1993**, *144*, 175. (f) Haruta, M.; Date, M. *Appl. Catal., A* **2001**, *222*, 427. (g) Iizuka, Y.; Fujiki, H.; Yamauchi, N.; Chijiiwa, T.; Arai, S.; Tsubota, S.; Haruta, M. *Catal. Today* **1997**, *36*, 115. (h) Okumura, M.; Coronado, J. M.; Soria, J.; Haruta, M.; Conesa, J. C. *J. Catal.* **2001**, *203*, 168.
(3) (a) Valden, M.; Lai, X.; Goodman, D. W. *Science* **1998**, *281*, 1647. (b) Meier, D. C.; Goodman, D. W. *J. Am. Chem. Soc.* **2004**, *126*, 1892. (c) Chen, M. S.; Goodman, D. W. *Science* **2004**, *306*, 252. (d) Chen, M.; Cai, Y.; Yan, Z.; Goodman, D. W. *J. Am. Chem. Soc.* **2006**, *128*, 6341.
(4) (a) Wallace, W. T.; Whetten, R. L. *J. Am. Chem. Soc.* **2002**, *124*, 7499. (b) Wallace, W. T.; Wyrwas, R. B.; Whetten, R. L.; Mitrić, R.; Bonačić-Koutecký, V. *J. Am. Chem. Soc.* **2003**, *125*, 8408.
(5) (a) Yoon, B.; Häkkinen, H.; Landman, U.; Wörz, A. S.; Antonietti, J.-M.; Abbet, S.; Judai, K.; Heiz, U. *Science* **2005**, *307*, 403. (b) Sanchez, A.; Abbet, S.; Heiz, U.; Schneider, W.-D.; Häkkinen, H.; Barnett, R. W.; Landman, U. *J. Phys. Chem. A* **1999**, *103*, 9573. (c) Häkkinen, H.; Abbet, S.; Sanchez, A.; Heiz, U.; Landman, U. *Angew. Chem., Int. Ed.* **2003**, *42*, 1297. (d) Yoon, B.; Häkkinen, H.; Landman, U. *J. Phys. Chem. A* **2003**, *107*, 4066. (e) Ricci, D.; Bongiorno, A.; Pacchioni, G.; Landman, U. *Phys. Rev. Lett.* **2006**, *97*, 036106.
(6) Remediakis, I. N.; Lopez, N.; Nørskov, J. K. *Angew. Chem., Int. Ed.* **2005**, *44*, 1824.
(7) (a) Guzman, J.; Gates, B. C. *J. Am. Chem. Soc.* **2004**, *126*, 2672. (b) Guzman, J.; Carrettin, S.; Corma, A. *J. Am. Chem. Soc.* **2005**, *127*, 3286.
(8) (a) Fu, L.; Wu, N. Q.; Yang, J. H.; Qu, F.; Johnson, D. L.; Kung, M. C.; Kung, H. H.; Dravid, V. P. *J. Phys. Chem. B* **2005**, *109*, 3704. (b) Hutchings, G. J.; Hall, M. S.; Carley, A. F.; Landon, P.; Solsona, B. E.; Kiely, C. J.; Herzing, A.; Makkee, M.; Moulijn, J. A.; Overweg, A.; Fierro-Gonzalez, J. C.; Guzman, J.; Gates. B. C. *J. Catal.* **2006**, *242*, 71.
(9) (a) Ishida, T.; Haruta, M. *Angew. Chem., Int. Ed.* **2007**, *46*, 7154. (b) Thompson, D. T. *Nanotoday* **2007**, *2*, 40. (c) Hashmi, A. S. K.; Hutchings, G. J. *Angew. Chem., Int. Ed.* **2006**, *45*, 7896.
(10) (a) Sanchez-Castillo, M. A.; Couto, C.; Kim, W. B.; Dumesic, J. A. *Angew. Chem., Int. Ed.* **2004**, *43*, 1140. (b) Liu, L. M.; McAllister, B.; Ye, H. Q.; Hu, P. *J. Am. Chem. Soc.* **2006**, *128*, 4017. (c) Shou, M.; Takekawa, H.; Ju, D. Y.; Hagiwara, T.; Lu, D. L.; Tanaka, K. *Catal. Lett.* **2006**, *108*, 119. (d) Kung, H. H.; Kung, M. C.; Costello, C. K. *J. Catal.* **2003**, *216*, 425. (e) Daté, M.; Haruta, M. *J. Catal.* **2001**, *201*, 221. (f) Daté, M.; Okumura, M.; Tsubota, S.; Haruta, M. *Angew. Chem., Int. Ed.* **2004**, *43*, 2129.
(11) (a) Schubert, M. M.; Hackenberg, S.; van Veen, A. C.; Muhler, M.; Plzak, V.; Behm, R. J. *J. Catal.* **2001**, *197*, 113. (b) Carrettin, S.; Concepción, P.; Corma, A.; Nieto, J. M. L.; Puntes, V. F. *Angew. Chem., Int. Ed.* **2004**, *43*, 2538. (c) Romero-Sarria, F.; Martinez, L. M.; Centeno, M. A.; Odriozola, J. A. *J. Phys. Chem. C* **2007**, *111*, 14469.
(12) (a) Grisel, R. J. H.; Nieuwenhuys, B. E. *J. Catal.* **2001**, *199*, 48. (b) Gluhoi, A. C.; Dekkers, M. A. P.; Nieuwenhuys, B. E. *J. Catal.* **2003**, *219*, 197.

(13) Matthey, D.; Wang, J. G.; Wendt, S.; Matthiesen, J.; Schaub, R.; Lægsgaard, E.; Hammer, B.; Besenbacher, F. *Science* **2007**, *315*, 1692.
(14) (a) Hernández, N. C.; Sanz, J. F.; Rodriguez, J. A. *J. Am. Chem. Soc.* **2006**, *128*, 15600. (b) Rashkeev, S. N.; Lupini, A. R.; Overbury, S. H.; Pennycook, S. J.; Pantelides, S. T. *Phys. Rev. B* **2007**, *76*, 035438.
(15) (a) Molina, L. M.; Rasmussen, M. D.; Hammer, B. *J. Chem. Phys.* **2004**, *120*, 7673. (b) Rasmussen, M. D.; Molina, L. M.; Hammer, B. *J. Chem. Phys.* **2004**, *120*, 988. (c) Molina, L. M.; Hammer, B. *J. Catal.* **2005**, *233*, 399. (d) Molina, L. M.; Hammer, B. *Appl. Catal., A* **2005**, *291*, 21.
(16) Zhang, C.; Yoon, B.; Landman, U. *J. Am. Chem. Soc.* **2007**, *129*, 2228.
(17) (a) Lopez, N.; Nørskov, J. K. *J. Am. Chem. Soc.* **2002**, *124*, 11262. (b) Mavrikakis, M.; Stoltze, P.; Nørskov, J. K. *Catal. Lett.* **2000**, *64*, 101. (c) Remediakis, I. N.; Lopez, N.; Nørskov, J. K. *Appl. Catal., A* **2005**, *291*, 13. (d) Lopez, N.; Nørskov, J. K.; Janssens, T. V. W.; Carlsson, A.; Puig-Molina, A.; Clausen, B. S.; Grunwaldt, J.-D. *J. Catal.* **2004**, *225*, 86. (e) Lopez, N.; Janssens, T. V. W.; Clausen, B. S.; Xu, Y.; Mavrikakis, M.; Bligaard, T. *J. Catal.* **2004**, *223*, 232. (f) Janssens, T. V. W.; Clausen, B. S.; Hvolbæk, B.; Falsig, H.; Christensen, C. H.; Bligaard, T.; Nørskov, J. K. *Top. Catal.* **2007**, *44*, 15. (g) Hvolbæk, B.; Janssens, T. V. W.; Clausen, B. S.; Falsig, H.; Christensen, C. H.; Nørskov, J. K. *Nanotoday* **2007**, *2*, 14.
(18) (a) Liu, Z.-P.; Hu, P.; Alavi, A. *J. Am. Chem. Soc.* **2002**, *124*, 14770. (b) Liu, Z.-P.; Gong, X.-Q.; Kohanoff, J.; Sanchez, C.; Hu, P. *Phys. Rev. Lett.* **2003**, *91*, 266102.
(19) Lemire, C.; Meyer, R.; Shaikhutdinov, S.; Freund, H.-J. *Angew. Chem., Int. Ed.* **2004**, *43*, 118.
(20) Zielasek, V.; Jürgens, B.; Schulz, C.; Biener, J.; Biener, M. M.; Hamza, A. V.; Bäumer, M. *Angew. Chem., Int. Ed.* **2006**, *45*, 8241.
(21) (a) Sinha, A. K.; Seelan, S.; Tsubota, S.; Haruta, M. *Angew. Chem.* **2004**, *116*, 1572. (b) Sinha, A. K.; Seelan, S.; Tsubota, S.; Haruta, M. *Angew. Chem., Int. Ed.* **2004**, *43*, 1546. (c) Hayashi, T.; Tanaka, K.; Haruta, M. *J. Catal.* **1998**, *178*, 566. (d) Nijhuis, T. A. R.; Visser, T.; Weckhuysen, B. M. *Angew. Chem.* **2005**, *117*, 1139. (e) Nijhuis, T. A. R.; Visser, T.; Weckhuysen, B. M. *Angew. Chem., Int. Ed.* **2005**, *44*, 1115.
(22) (a) Abad, A.; Concepción, P.; Corma, A.; Garcia, H. *Angew. Chem., Int. Ed.* **2005**, *44*, 4066. (b) Chang, F. W.; Yu, H. Y.; Roselin, L. S.; Yang, H. C.; Ou, T. C. *Appl. Catal., A* **2006**, *302*, 157. (c) Liu, Z.-P.; Jenkins, S. J.; King, D. A. *Phys. Rev. Lett.* **2005**, *94*, 196102. (d) Idakiev, V.; Tabakova, T.; Naydenov, A.; Yuan, Z. Y.; Su, B. L. *Appl. Catal., B* **2006**, *63*, 178. (e) Tabakova, T.; Idakiev, V.; Tenchev, K.; Boccuzzi, F.; Manzoli, M.; Chiorina, A. *Appl. Catal., B* **2006**, *63*, 94. (f) Fu, Q.; Saltsburg, H.; Flytzani-Stephanopoulos, M. *Science* **2003**, *301*, 935.
(23) (a) Kondo, Y.; Takayanagi, K. *Science* **2000**, *289*, 606. (b) Oshima, Y.; Onga, A. *Phys. Rev. Lett.* **2003**, *91*, 205503.
(24) (a) Tosatti, E.; Prestipino, S.; Kostlmeier, S.; Dal Corso, A.; Di Tolla, F. D. *Science* **2001**, *291*, 288. (b) Bilalbegović, G. *Phys. Rev. B* **1998**, *58*, 15412.
(25) (a) Delley, B. *J. Chem. Phys.* **1990**, *92*, 508. (b) Delley, B. *J. Chem. Phys.* **2003**, *113*, 7756. DMol^3 is available from Accelrys.
(26) Perdew, J. P.; Burke, K.; Ernzerhof, M. *Phys. Rev. Lett.* **1996**, *77*, 3865.
(27) Monkhorst, H. J.; Pack, J. D. *Phys. Rev. B* **1976**, *13*, 5188.
(28) (a) Henkelman, G.; Jonsson, H. *J. Chem. Phys.* **2000**, *113*, 9978. (b) Olsen, R. A.; Kroes, G. J.; Henkelman, G.; Arnaldsson, A.; Jonsson, H. *J. Chem. Phys.* **2004**, *121*, 9776.
(29) (a) Ijima, S. *Nature* **1991**, *354*, 56. (b) Saito, R.; Fujita, M.; Dresselhaus, G.; Dresselhaus, M. S. *Appl. Phys. Lett.* **1992**, *60*, 2204.
(30) (a) Mills, G.; Gordon, M. S.; Metiu, H. *J. Chem. Phys.* **2003**, *118*, 4198. (b) Varganov, S. A.; Olson, R. M.; Gordon, M. S.; Metiu, H. *J. Chem. Phys.* **2003**, *119*, 2531. (c) Mills, G.; Gordon, M. S.; Metiu, H. *Chem. Phys. Lett.* **2002**, *359*, 493.
(31) (a) Weiher, N.; Beesley, A. M.; Tsapatsaris, N.; Delannoy, L.; Louis, C.; van Bokhoven, J. A.; Schroeder, S. L. M. *J. Am. Chem. Soc.* **2007**, *129*, 2240. (b) Schaub, R.; Wahlström, E.; Rønnau, A.; Lægsgaard, E.; Stensgaard, I.; Besenbacher, F. *Science* **2003**, *299*, 377. (c) Waholström, E.; Vestergaard, E. K.; Schaub, R.; Vestergaard, M.; Lægsgaard, E.; Stensgaard, I.; Besenbacher, F. *Science* **2004**, *303*, 511. (d) van Bokhoven, J. A.; Louis, C.; Miller, J. T.; Tromp, M.; Safonova, O. V.; Glatzel, P. *Angew. Chem., Int. Ed.* **2006**, *45*, 4651.
(32) Deng, X.; Min, B. K.; Guloy, A.; Friend, C. M. *J. Am. Chem. Soc.* **2005**, *127*, 9267.
(33) Hüber, H.; McIntosh, D.; Ozin, G. A. *Inorg. Chem.* **1977**, *16*, 975.

NL072409T